Bull. Korean Chem. Soc. 2014, Vol. 35, No. 4 1229
http://dx.doi.org/10.5012/bkcs.2014.35.4.1229

Strong Light-Matter Interaction in ZnO Nanowires

So Hyeong Sohn, Seulki Lee,† Noh Soo Han, Yong Jin Park, Seung Min Park, Myong Yong Choi,† and Jae Kyu Song*

*Department of Chemistry, Kyung Hee University, Seoul 130-701, Korea. *E-mail: jaeksong@khu.ac.kr*
†Department of Chemistry and Research Institute of Natural Science, Gyeongsang National University, Jinju 660-701, Korea
Received December 13, 2013, Accepted December 24, 2013

Key Words : Zinc oxide, Nanowire, Photonic confinement, Light-matter interaction, Polariton

Zinc oxide (ZnO) has been investigated for UV/blue emitters and optoelectronics because of its wide band gap energy (3.37 eV).[1-3] In addition, several interesting properties are observed in ZnO. First, the large exciton binding energy and oscillator strength result in the primary excitation of the excitons at room temperature.[4,5] Second, light is efficiently guided for the photonic confinement in nanowires.[6-8] Another property is the quantum mechanical light-matter interaction between a travelling photon and exciton,[9-11] which is much more intense compared to other semiconductors. Moreover, the light-matter interaction is enhanced in nanowires due to the confined mode volume and the enhanced oscillator strength.[6-11] Thus, a strong exciton-photon coupling leads to the exciton-polariton in the nanowires, where the optical properties are not only determined by the electronic states but also by the geometries and dimensions.

Among the various nanostructures of ZnO, the most extensively investigated are one-dimensional nanowires due to their natural cavity mode and optical gain.[1-5] In addition, the active guiding of light takes place in nanowires because the vacuum wavelength of the guided light is longer than the wire diameter. However, the light-matter interaction has not been well understood in the nanowaveguide of ZnO. In this Note, we study the light-matter interaction in ZnO nanowires. The abnormal spectral spacing of Fabry–Pérot-type modes was observed in the isolated single nanowire, which indicated the strong exciton-photon coupling in a nanocavity. The lasing modes became blue-shifted with increase in the excitation intensity, which implied the weakening of the exciton states and thus the reduction of the light-matter interaction. At the high excitation intensity, additional lasing modes were observed in the low energy regime, which was attributed to the formation of electron-hole plasma state and band gap renormalization. The lasing in the electron-hole plasma state was also explained by the light-matter interaction in nanowires.

The typical photoluminescence spectrum of ZnO nanowires is presented in the inset of Figure 1(a), which was obtained at the excitation intensity of 10 μJ/cm^2. The UV peak at 3.25 eV indicated the exciton state emission.[1-3] The nearly absent visible emission (2-3 eV) suggested that the defect states were minimized in the nanowires.[4,5] The emission spectra of the single nanowire were also obtained as a function of the excitation intensity to investigate the photonic confinement effect. The sharp peak (mode **a**) was observed

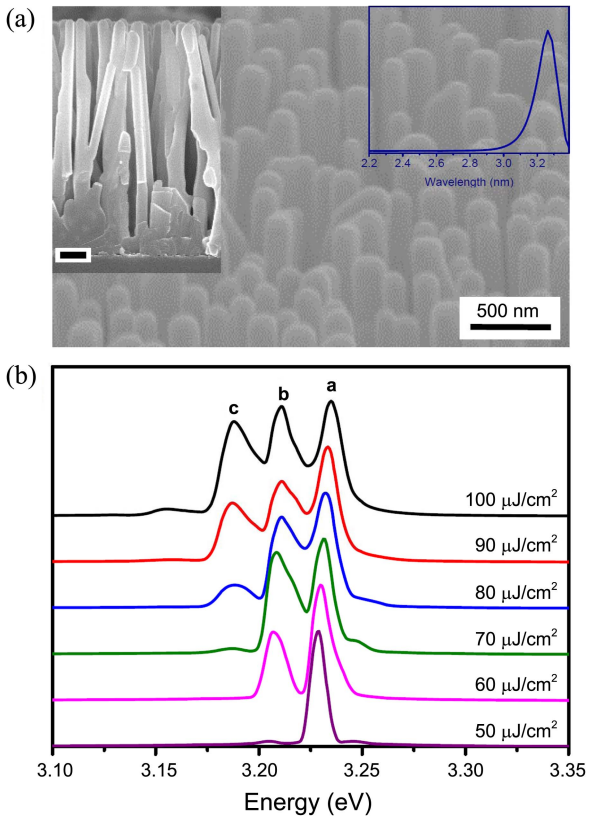

Figure 1. (a) A scanning electron microscopy (SEM) image of ZnO nanowires. The left inset shows an SEM image of the cross section of ZnO nanowires. The scale bar is 500 nm. The right inset shows the photoluminescence spectrum of ZnO nanowires, which presents the UV peak at 3.25 eV and nearly absent visible emission (2-3 eV). (b) The emission spectra of a single nanowire were obtained with increasing excitation intensity. The sharp lasing peak (mode **a**) appears in the normal band gap at the lasing threshold (50 μJ/cm^2). The lasing modes in the renormalized band gap (mode **b** and **c**) gain intensities, as the excitation intensity is further increased into the electron-hole plasma regime. The peak positions of the individual modes are blue-shifted with increasing excitation intensity.

at the excitation intensity of 50 μJ/cm^2 (Figure 1(b)), where the bandwidth of the peak was reduced by ~20 times compared to the normal emission band. This narrow band indicated that the lasing threshold was 50 μJ/cm^2 in this nanowire.[12,13] With increase in the excitation intensity above the lasing threshold, new sharp peaks (modes **b** and **c**) appeared in the lower energy regime, which were attributed

to Fabry–Pérot-type lasing modes in the renormalized band gap.[14,15] In general, the Coulomb interactions between an electron and hole in the exciton state become screened and the exciton binding energy gradually reduced with increase in the carrier density. At a Mott density, electrons and holes are only weakly correlated and the exciton states are not stable due to the screened interaction. Above the Mott density, electron–hole plasma states are formed and the band gap is renormalized.[14,15] In other words, the emission in the electron–hole plasma states is red-shifted with increasing carrier density. Accordingly, the reduced band gap in the electron–hole plasma states was responsible for the appearance of the Fabry–Pérot modes in the lower energy regime at the high excitation intensity (Figure 1(b)). In addition, the lasing in the normal band gap (mode **a**) decreased with further increase in the excitation intensity (> 80 μJ/cm^2) due to the red-shift of the emission band in the electron–hole plasma states (Figure 2(a)). Instead, other Fabry–Pérot modes (**b** and **c**) in the reduced band gap gained intensities, while the overall intensity of the lasing modes increased superlinearly.

The spectral spacing of lasing modes has often been used to determine the optical cavity length. The cavity length (L) was first calculated by the classical cavity model, $\Delta\nu = c/2nL$,[4,10] where $\Delta\nu$ is the frequency difference between the lasing modes, c is the speed of light in vacuum, and n is the refractive index of ZnO (2.4). However, the calculated cavity length (11 μm) from the spectral spacing ($\Delta\nu$ = 5.5 THz) was much longer than the nanowire lengths (≤ 4 μm). Indeed, the total internal reflection in the waveguide could allow a longer travel length than a cavity length. The large difference in the refractive index between the cavity and air could result in a travel length of up to 9.6 μm for a 4.0 μm-long nanowire, which still did not explain the calculated cavity length. In addition, the spectral spacing in Figure 2(b) was not the same because the energy difference between modes **a** and **b** was 22 meV and the difference between modes **b** and **c** was 24 meV.

The non-classical and non-identical spectral spacing indicated strong light-matter interactions in the nanowires. Since the coupling strength between a photon and an exciton is related to the oscillator strength and the mode volume, a strong exciton-photon coupling is expected in the nanowires. In the exciton-polariton regime, the wavevector ($\boldsymbol{k}$) is correlated to the energy of the polariton, $E(\omega, k)$,[9,11]

$$E(\omega, k) = \hbar\omega = \frac{\hbar ck}{\sqrt{\varepsilon(\omega)}} \quad (1)$$

where ω is the angular frequency, $\varepsilon(\omega)$ is the dielectric function of the medium, and k is $\sqrt{k_x^2 + k_y^2 + k_z^2}$. Thus, the confined photon in a nano-cavity deviated considerably from the classical theory, because the energy of the polariton is closely correlated to $\varepsilon(\omega)$. For example, the group velocity of the confined photons was slowed down by a factor of seven in a CdS cavity near the resonance energy due to the exciton-photon coupling,[7,8] which explained the mismatch of the nanowire length to the cavity length obtained by the classical theory. Indeed, the cavity length was reasonably estimated to be 3.9 μm, when the group velocity in the ZnO nanowires was assumed to be one seventh of the speed of light. Therefore, the non-classical spectral spacing implied

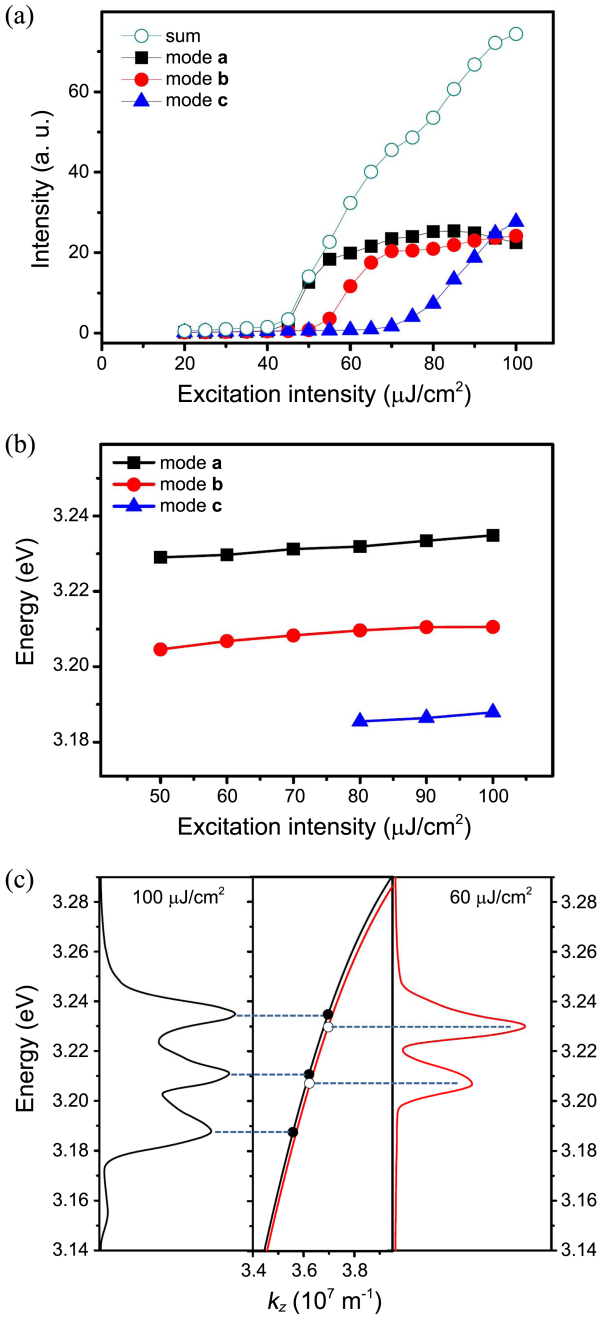

Figure 2. (a) The integrated emission intensities of the individual modes are presented as a function of the excitation intensity. The integrated intensity increases superlinearly above the lasing threshold (50 μJ/cm^2). (b) The peak energies of the individual modes increase with increase in the excitation intensity. (c) The energy–wavevector diagrams in the exciton-polariton model are plotted as a function of k_z, which denotes the parallel wavevector to the long axis of the nanowire (center). The lasing emission spectrum at 100 μJ/cm^2 matches with the dispersion curve (black) of the 2.9-fold enhanced oscillator strength (left). The lasing emission spectrum at 60 μJ/cm^2 matches with the dispersion curve (red) of the 3.2-fold enhanced oscillator strength at the same wavevectors (right).

the presence of strong light-matter interactions in the nanowire.

In the exciton-polariton model, $\varepsilon(\omega)$ is described as follows,[9,11]

$$\varepsilon(\omega) = \varepsilon_{\infty}\left(1 + \sum_{j=A,B,C} \Omega_j \frac{\omega_{j,L}^2 - \omega_{j,T}^2}{\omega_{j,T}^2 - \omega^2 - i\omega\gamma_j}\right) \quad (2)$$

where ε_{∞} is the background dielectric constant, γ is the damping constant, Ω is the prefactor, ω_T and ω_L are the transverse and longitudinal resonance frequencies, respectively. Thus, $\varepsilon(\omega)$ increased steeply and the group velocity of the confined photons was significantly reduced as the energy of the polariton approached the resonance energy. As a result, the polariton dispersion curve in the energy-wavevector diagram became flattened near the resonance energy (Figure 2(c)). The curved dispersion was responsible for the smaller energy difference between modes **a** and **b**, despite the same interval of the wavevector, than the difference between modes **b** and **c**. Therefore, the non-identical spectral spacing of the Fabry-Pérot modes was also attributed to the strong light-matter interaction.

Upon closer examination of Figure 1(b), the peak positions of the individual modes were blue-shifted with increasing excitation intensity, which was more clearly presented in Figure 2(b). The exciton binding energy was reduced by the carrier screening at the high carrier density, which weakened the exciton states and the exciton-photon coupling.[14-16] Thus, the blue-shift of the mode was correlated to the less enhanced oscillator strength at the high carrier density. Indeed, the polariton dispersion curves (Figure 2(c)) obtained with different enhancement factors clarified the blue-shift. When the oscillator strength was 3.2-fold enhanced compared to the bulk, the dispersion curve (red solid line) corresponded to the lasing emission spectrum at 60 μJ/cm^2. On the other hand, the lasing spectrum at 100 μJ/cm^2 was matched with the dispersion curve of the 2.9-fold enhanced oscillator strength (black solid line) at the same wavevectors. Accordingly, the blue-shift indicated the decrease in the enhancement factor and the exciton-photon coupling.

Remarkably, the energy-wavevector diagram of the exciton-polariton model was also applicable to the electron–hole plasma states, where the exciton states were not stable and electrons and holes were only weakly correlated. The lasing modes in the renormalized band gap were attributed to Fabry–Pérot-type modes in the electron–hole plasma states (Figure 1(b)).[14,15] Indeed, a recent many-body theory considered the screened electron–hole interactions, Coulomb-repulsions, and band gap renormalization, which pointed out that the dispersion curve in the electron–hole plasma states was also strongly curved.[17] Moreover, the energy-wavevector diagram in the electron–hole plasma states was phenomenologically similar to that in the exciton-polariton model. Therefore, the non-classical, non-identical spectral spacing and the blue-shift of the Fabry–Pérot modes at the high carrier density regime indicated significant light-matter interactions even in the electron–hole plasma states. It is noted that the light-matter interaction in the electron–hole plasma states turned out to be weaker than that in the exciton states (Figure 2(c)), which reduced the enhancement factors compared to the exciton states.

In summary, strong quantum mechanical light-matter interaction was observed in ZnO nanowires. The non-classical and non-identical spectral spacing of Fabry–Pérot lasing modes resulted from the strong exciton-photon coupling in nanowires, which was explained by the exciton-polariton model. The lasing modes were blue-shifted at the high carrier density, which was correlated with the weakening of the exciton states. The light-matter interaction still played an important role in the electron-hole plasma states, although the strength was weaker than the exciton states.

Experimental Sections

The details of ZnO nanowire synthesis and optical measurements have been reported elsewhere.[16,18] The sol-gel solutions of ZnO were prepared by dissolving zinc acetate dihydrate ($Zn(CH_3COO)_2{\cdot}2H_2O$) in methanol and mixing with monoethanolamine at a volume ratio of 1:5. The seed layers were prepared by spin coating of sol-gel solutions onto silicon wafer substrates, where ZnO nanowires were grown by a chemical vapor transport method. The source mixture of Zn (1.0 g) and ZnO (1.0 g) was placed in an alumina boat and loaded inside a horizontal tube furnace. The seed film was placed 40 mm downstream of the source boat, where the temperature was 820 °C. The growth was carried out under flow of N_2 (140 sccm) and O_2 (5 sccm) for 10 min. The shapes and lengths of the nanostructures were characterized by scanning electron microscopy. The diameters of the nanowires were 200-250 nm and the lengths were in the range of 3-4 mm (Figure 1(a)). The nanowires were sonicated in methanol to isolate individual nanowires and drop coated onto silicon wafer substrates. An isolated single nanowire was selectively excited by 355 nm through an ultraviolet microscope objective. The normal photoluminescence and lasing emissions were collected by the same objective, resolved spectrally by a monochromator, and detected by a photomultiplier.

Acknowledgments. This research was supported by Basic Science Research Program through the National Research Foundation of Korea (NRF) funded by the Ministry of Education, Science and Technology (NRF-2012R1A1A 2039882). This work was also supported by the National Research Foundation of Korea Grant funded by the Korean Government (MEST, NRF-2009-C1AAA001-0092939).

References

1. Huang, M. H.; Mao, S.; Feick, H.; Yan, H.; Wu, Y.; Kind, H.; Weber, E.; Russo, R.; Yang, P. *Science* **2001**, *292*, 1897.
2. Özgür, Ü.; Alivov, Y. I.; Liu, C.; Teke, A.; Reshchikov, M. A.; Doğan, S.; Avrutin, V.; Cho, S.-J.; Morkoç, H. *J. Appl. Phys.* **2005**, *98*, 041301.

3. Klingshirn, C. *Phys. Status Solidi B* **2007**, *9*, 3027.
4. Johnson, J. C.; Knutsen, K. P.; Yan, H.; Law, M.; Zhang, Y.; Yang, P.; Saykally, R. J. *Nano Lett.* **2004**, *4*, 197.
5. Song, J. K.; Szarko, J. M.; Leone, S. R.; Li, S.; Zhao, Y. *J. Phys. Chem. B* **2005**, *109*, 15749.
6. van Vugt, L. K.; Zhang, B.; Piccione, B.; Spector, A. A.; Agarwal, R. *Nano Lett.* **2009**, *9*, 1684.
7. Piccione, B.; van Vugt, L. K.; Agarwal, R. *Nano Lett.* **2010**, *10*, 2251.
8. van Vugt, L. K.; Piccione, B.; Agarwal, R. *Appl. Phys. Lett.* **2010**, *97*, 061115.
9. van Vugt, L. K.; Rühle, S.; Ranvindran, P.; Gerritsen, H. C.; Kuipers, L.; Vanmaekelbergh, D. *Phys. Rev. Lett.* **2006**, *97*, 147401.
10. van Vugt, L. K.; Rühle, S.; Vanmaekelbergh, D. *Nano Lett.* **2006**, *6*, 2707.
11. Vanmaekelbergh, D.; van Vugh, L. K. *Nanoscale* **2011**, *3*, 2783.
12. Johnson, J. C.; Yan, H.; Yang, P.; Saykally, R. J. *J. Phys. Chem. B* **2003**, *107*, 8816.
13. Maslov, A. V.; Ning, C. Z. *Appl. Phys. Lett.* **2003**, *83*, 1237.
14. Bagnall, D. M.; Chen, Y. F.; Zhu, Z.; Yao, T.; Shen, M. Y.; Goto, T. *Appl. Phys. Lett*. **1998**, *73*,1038.
15. Yamamoto, A.; Kido, T.; Goto, T.; Chen, Y.; Yao, T.; Kasuya, A. *Appl. Phys. Lett*. **1999**, *75*, 469.
16. Han, N. S.; Shim, H. S.; Lee, S.; Park, S. M.; Choi, M. Y.; Song, J. K. *Phys. Chem. Chem. Phys.* **2012**, *14*, 10556.
17. Versteegh, M. A. M.; Kuis, T.; Stoof, H. T. C.; Dijkhuis, J. I. *Phys. Rev. B* **2011**, *84*, 035207.
18. Shim, H. S.; Seo, J. H.; Han, N. S.; Park, S. M.; Sohn, Y.; Kim, C.; Song, J. K. *Bull. Korean Chem. Soc.* **2012**, *33*, 1075.